Protein and DNA Residue Orientations in the Filamentous Virus Pf1 Determined by Polarized Raman and Polarized FTIR Spectroscopy†

Masamichi Tsuboi,‡ Yoshiko Kubo,§ Teruki Ikeda,§ Stacy A. Overman, Olivia Osman, and George J. Thomas, Jr.*

Division of Cell Biology and Biophysics, School of Biological Sciences, University of Missouri-Kansas City, Kansas City, Missouri 64110

Received September 3, 2002

ABSTRACT: The *Pseudomonas* bacteriophage Pf1 is a long (∼2000 nm) and thin (∼6.5 nm) filament consisting of a covalently closed, single-stranded DNA genome of 7349 nucleotides coated by 7350 copies of a 46-residue α-helical subunit. The coat subunits are arranged as a superhelix of $C_1S_{5.4}$ symmetry (class II). Polarized Raman and polarized FTIR spectroscopy of oriented Pf1 fibers show that the packaged single-stranded DNA genome is ordered specifically with respect to the capsid superhelix. Bases are nonrandomly arranged along the capsid interior, deoxynucleosides are uniformly in the C2′-endo/anti conformation, and the average DNA phosphodioxy group (PO_2^-) is oriented so that the line connecting the oxygen atoms (O···O) forms an angle of 71° ± 5° with the virion axis. Raman and infrared amide band polarizations show that the subunit α-helix axis is inclined at an average angle of 16° ± 4° with respect to the virion axis. The α-helical symmetry of the capsid subunit is remarkably rigorous, resulting in splitting of Raman-active helix vibrational modes at 351, 445 and 1026 cm^{-1} into apparent *A*-type and E_2-type symmetry pairs. The subunit tyrosines (Tyr 25 and Tyr 40) are oriented with phenoxyl rings packed relatively close to parallel to the virion axis. The Tyr 25 and Tyr 40 orientations of Pf1 are surprisingly close to those observed for Tyr 21 and Tyr 24 of the Ff virion (C_5S_2 symmetry, class I), suggesting a preferred tyrosyl side chain conformation in packed α-helical subunits, irrespective of capsid symmetry. The polarized Raman spectra also provide information on the orientations of subunit alanine, valine, leucine and isoleucine side chains of the Pf1 virion.

Bacteriophage Pf1 is a long and thin flexible filament (∼2000 nm × 6.5 nm) that infects *Pseudomonas aeruginosa* strain K. Pf1 is about twice the length of other well characterized filamentous bacteriophages, including the *Pseudomonas* phage Pf3 and the coliphages Ff, IKe, and If1 (*1*). Among these filamentous phages, Pf1 forms the most highly ordered fibers and has been the most amenable to fiber X-ray diffraction analysis (*2*, *3*). Dilute liquid crystals of Pf1 are also highly effective in the alignment of macromolecules to facilitate measurement of residual dipolar couplings that improve NMR structure determinations (*4*, *5*). The high degree of alignment achievable for Pf1 in fiber and liquid crystalline states (*6*) makes it a favorable target for polarized spectroscopic examinations. Like other filamentous bacteriophages, Pf1 is also an attractive model to study nucleoprotein assembly and membrane transport.

The mature Pf1 virion comprises a single-stranded (ss) and covalently closed DNA genome of 7349 nucleotides sheathed by 7350 copies of a 46-residue α-helical subunit (sequence ^{1}GVIDTSAVES ^{11}AITDGQGDMK ^{21}AIGGYIVGAL ^{31}VILAVAGLIY ^{41}SMLRKA) (*1*). A few copies of minor proteins cap the filament ends. The structure of Pf1 has been investigated by a variety of diffraction and spectroscopic methods (*2*, *3*, *7*−*19*). Plausible structural models incorporate a completely α-helical subunit, the helix axis of which is inclined at a small angle from the virion axis and with the N-terminus at the outer surface of the tubular capsid and the C-terminus at the interior (*3*, *15*, *16*, *19*). The viral genome, which occupies the core of the capsid, is presumed to form a loop spanning the full length of the filament. Day and co-workers (*16*, *20*, *21*) demonstrated that this is feasible if the ssDNA loop is highly extended along its full length so that the deoxyribose-phosphate moieties are positioned close to the virion axis and the DNA bases protrude outward toward the adjoining wall of the tubular capsid. In this model, termed *P* DNA (*16*), the nucleotides adopt the same deoxyribosyl conformation (C2′-endo/anti) that occurs in *B* DNA, but the proposed nucleotide axial repeat of *P* DNA (∼6 Å) is about 75% greater than that of *B* DNA. Raman and ultraviolet resonance Raman (UVRR)

† Part LXXIX in the series Structural Studies of Viruses by Raman Spectroscopy.

* To whom correspondence should be addressed. Telephone: 816-235-5247. Fax: 816-235-1503. E-mail: thomasgj@umkc.edu.

‡ Permanent address: College of Science and Engineering, Iwaki-Meisei University, Iwaki, Fukushima 970-8551, Japan.

§ Permanent address: JASCO, 2967-5 Ishikawa-cho, Hachioji, Tokyo 192-8537, Japan.

[1] Abbreviations: Pf1, a class II filamentous virus; Pf3, a class II filamentous virus; Ff, a class I filamentous virus (includes strains fd, f1, and M13); ss, single-stranded; FTIR, Fourier transform infrared; UVRR, ultraviolet-resonance Raman; *D*, infrared dichroic ratio, equal to the quotient of absorbances of radiation polarized parallel ($A_{\parallel}$) and perpendicular ($A_{\perp}$) to a specified axis; (θ, χ), Eulerian angles defining the orientation of the Raman tensor coordinates (*x*, *y*, *z*) with respect to the laboratory coordinates (*a*, *b*, *c*); θ_h, tilt angle of subunit α-helix axis with respect to virion capsid axis; χ^1, side-chain torsion angle defined by atoms N−C^{α}−C^{β}−C^{γ} of tryptophan; $\chi^{2,1}$, side-chain torsion angle defined by atoms C^{α}−C^{β}−C^{γ}−$C^{\delta 1}$ of tryptophan.

10.1021/bi020566v CCC: $25.00
Published on Web 01/03/2003

markers of the packaged Pf1 DNA molecule indicate that the nucleotides indeed incorporate the C2′-endo/anti deoxyribosyl conformation, that the base moieties are neither paired nor stacked with one another, and that the base exocyclic groups are highly reactive to Hg(II) ions (*11*). These local structural characteristics are compatible with the *P*-DNA model (*10*, *17*). Additional biochemical and spectroscopic data in support of this model have been discussed (*11*, *14*, *15*). Interestingly, the highly extended Pf1 DNA structure proposed by Day and co-workers (*16*) has also been suggested as a prototype for DNA molecules subjected to high mechanical or torsional stress (*22*, *23*). Further details regarding the conformation of the packaged Pf1 DNA genome, the orientations of capsid subunit side chains, and the possible interactions occurring between protein and DNA within the virion assembly remain largely unresolved.

The methods of vibrational spectroscopy employed here—polarized Raman and polarized Fourier transform infrared (FTIR) spectroscopy—are capable of providing additional structural information at the molecular level on subunit and DNA components of the Pf1 assembly. Other applications of polarized Raman methods to the filamentous viruses Ff (strains fd and f1) and Pf1 have been described (*19*, *24*−*28*) and reviewed elsewhere (*29*, *30*). The use of polarized infrared spectroscopy to study oriented gels of Ff and Pf1 virions has also been reported (*9*, *31*). In the case of the Ff assembly exhaustive residue-specific isotope substitutions and selective site-specific mutations (*32*−*36*) have established definitive vibrational band assignments for viral protein and DNA constituents. These enable more effective use of the polarized spectroscopic methods for detailed structural interpretations and many of the assignments established previously for the Ff assembly are exploited here in polarized Raman and FTIR analyses of the Pf1 assembly.

EXPERIMENTAL METHODS

1. Sample Preparation. Stocks of wild-type Pf1 and the host *Pseudomonas aeruginosa* strain K were obtained originally from Dr. Loren A. Day, Public Health Research Institute, New York. Growth media and standard reagents were obtained from Sigma Chemical (St. Louis, MO) and Fisher Scientific (St. Louis, MO). The virus was grown in MS medium containing 1% glucose and 4 mM $CaCl_2$. Mature viral particles, extruded through the bacterial cell membrane and into the growth medium, were collected by precipitation with poly(ethylene glycol) (2%) and NaCl (0.5 M), followed by low-speed centrifugation. The virus precipitate was resuspended in 10 mM Tris (pH 7.8 ± 0.2), and the resulting suspension was purified by four cycles of pelleting at 330 000*g* for 1.5 h and resuspension of the pellet in 10 mM Tris buffer, pH 7.8. This procedure accomplishes essentially complete removal of excess NaCl and is conducive to the formation of highly oriented fibers (*4*, *19*). Typically, 20−30 mg of purified virus was obtained from a 1 L preparation. Pf1 concentration was determined by UV spectrophotometry using an extinction coefficient at 270 nm of 2.06 mL mg^{-1} cm^{-1} (*15*, *37*).

Oriented Pf1 fibers of ∼0.5 mm thickness were prepared for polarized Raman measurement by slowly drawing a droplet of Pf1 solution (∼100 μg/μL in 10 mM Tris, pH 7.8) in a fiber pulling device maintained at 20 °C and 92% relative humidity (*25*). An oriented Pf1 fiber in its hygrostatic and thermostatic chamber was placed on the microscope stage of the Raman microspectrophotometer for subsequent polarized Raman measurements. Oriented Pf1 films of about 0.1 mm thickness were prepared for polarized FTIR measurements by unidirectional stroking of the Pf1 solution over an area of about 7 mm × 20 mm on a CaF_2 plate at 20 °C. The film was maintained at a constant relative humidity of 92% using a custom designed hygrostatic chamber (*38*). Fibers and films were scanned in a polarizing light microscope to identify regions of the samples containing the greatest degree of virion orientation, as assessed by the uniformity and intensity of birefringent patterns. Optimally oriented samples were estimated to contain between 95% and 100% of the Pf1 particles oriented. A more detailed assessment has been described elsewhere (*25*).

2. Raman Microspectroscopy. Raman spectra were recorded on a Jasco NRS-2000 microspectrophotometer using 514.5 nm excitation from a NEC GL2162 argon ion laser. The laser power at the sample was maintained at 500 mW. The laser beam was directed through a 50X objective onto the fiber through a cover glass which sealed the sample within the hygrostatic chamber. Backscattering (360°) was collected with the same objective, directed through a polarizing analyzer and an optical scrambler onto the entrance slit of a Czerny-Turner polychromator, and detected by a liquid nitrogen-cooled, back illuminated charge-coupled device (Princeton Instruments LN/CCD-1100PB). Additional data collections were made on a Jasco NRS-2100, which has the same microscope, polychromator, and detector as the Jasco NRS-2000.

Initially, the polarized Raman intensities I_{cc} and I_{cb} were measured by aligning the fiber along the front-to-rear direction of the microscope platform. These intensities correspond to the fiber tensor components *cc* and *cb*, respectively. Here, the *c*-axis is the fiber axis (also the virion axis), and the *b*-axis is perpendicular to *c*. The notation I_{cc} signifies that the electric vectors of both the exciting and scattered radiation are along *c*; similarly, I_{cb} signifies that the exciting and scattered electric vectors are along *c* and *b*, respectively. With the polarization analyzer adjusted so that only the *c* component of the scattered radiation entered the spectrometer, I_{cc} was recorded. A 90° rotation of the analyzer allowed I_{cb} to be recorded. Subsequent rotation of the fiber by 90° on the microscope platform allowed I_{bb} and I_{bc} to be measured in succession using the same procedure as above. If the laser beam is precisely focused on the same portion of the sample throughout this protocol, then we expect $I_{cb} = I_{bc}$, which was most often the case. Occasionally, however, we found that $I_{cb} \neq I_{bc}$, indicating imprecise positioning. To correct for this effect, we defined $I_{cc}^{corr} = (I_{cc}^{obs})(I_{bc}/I_{cb})$ and $I_{cb}^{corr} = (I_{cb}^{obs})(I_{bc}/I_{cb})$, where the quotient (I_{bc}/I_{cb}) modifies the observed polarized Raman intensity (I^{obs}) to yield a corrected value (I^{corr}). (For simplicity, we omit the superscript notation in all subsequent discussions and in the labeling of the figures shown below.)

3. Infrared Microspectroscopy. Infrared absorption spectra were measured on a Jasco FT/IR-300S spectrometer. For polarization measurements (infrared dichroism), the axis of orientation of the film (also the virion axis) and the direction of the electric vector of the polarized radiation were always placed at 45° with respect to the vertical line. This setting

enabled elimination of possible errors in the observed dichroic ratio due to the polarization of the optical system. For comparison with Pf1, polarized infrared spectra of the Ff virus (strain fd) were also examined. The oriented Ff films were prepared using the same procedure as those for Pf1 films and spectroscopic measurements were made using the same protocol.

4. Data Analysis. To each Raman band there corresponds a Raman tensor α, which is defined as the first derivative of the molecular polarizability with respect to the vibrational normal coordinate. The tensor component α_{ij} represents the polarizability change for radiation with incident and scattered electric vectors polarized, respectively, in the *i* and *j* directions. Here, we consider only the relative magnitudes of the principal (i.e., diagonal) tensor components, namely, $\alpha_{xx}/\alpha_{zz} \equiv r_1$ and $\alpha_{yy}/\alpha_{zz} \equiv r_2$ (*29*). Highly anisotropic Raman tensors are characterized by values of r_1 and/or r_2 differing greatly from unity, whereas isotropic tensors have $r_1 = r_2 = 1$. For Raman tensors that are axially symmetric with respect to *z*, $r_1 = r_2$. Tensor components associated with any vibration can be calculated from knowledge of the appropriate polarized Raman band intensities I_{kl}, where *k* and *l* (= *a*, *b*, *c*) are the directions of the incident and scattered electric vectors, respectively. Further details of the method have been given (*24*, *29*, *39*, *40*).

To each infrared band there corresponds a transition dipole moment vector μ, which is defined as the first derivative of the molecular dipole moment with respect to the vibrational normal coordinate. Polarized infrared radiation is absorbed by a vibrating molecule only if there is a nonzero component of μ (e.g., μ_i) in the same direction as that of polarization of the radiation. The absorption intensity of the corresponding infrared band is A_i. Here, we consider the ratio of absorption intensities $A_{||}/A_{\perp}$, which is the quotient of infrared absorption intensities for radiation that is polarized respectively parallel and perpendicular to the unique axis of molecular orientation in the sample. In the present case, this is the axis of the oriented film (*c*), which is also the virion axis. The quotient $A_{||}/A_{\perp}$ is defined as the dichroic ratio (*D*) of the infrared band in question. For randomly oriented molecules, each infrared absorption band should exhibit no dichroism, i.e., $A_{||} = A_{\perp}$. For an oriented film or fiber, an infrared band may exhibit parallel dichroism ($A_{||} > A_{\perp}$), perpendicular dichroism ($A_{||} < A_{\perp}$), or no dichroism ($A_{||} = A_{\perp}$), depending upon the direction of the transition dipole moment and its orientation with respect to the polarized infrared radiation. Further discussion of infrared dichroism in biological molecules has been given elsewhere (*41*, *42*).

RESULTS AND INTERPRETATION

1. Raman Bands of Pf1. The I_{cc} and I_{bb} polarized Raman spectra obtained from an oriented fiber of the Pf1 filamentous virus using 514.5 nm excitation are shown in Figure 1 (200−1170 cm^{-1} region) and Figure 2 (1100−1800 cm^{-1} region). Included in Figure 2 are the I_{cb} and I_{bc} polarizations which, as noted in the Experimental Methods section, permit correction for polarization errors due to possible imprecision in the 90° rotation of the fiber with respect to the electric vector of the exciting radiation. The data shown in Figures 1 and 2 confirm and extend the Raman spectra of Pf1 reported previously (*7*, *19*, *43*). The data are collected in

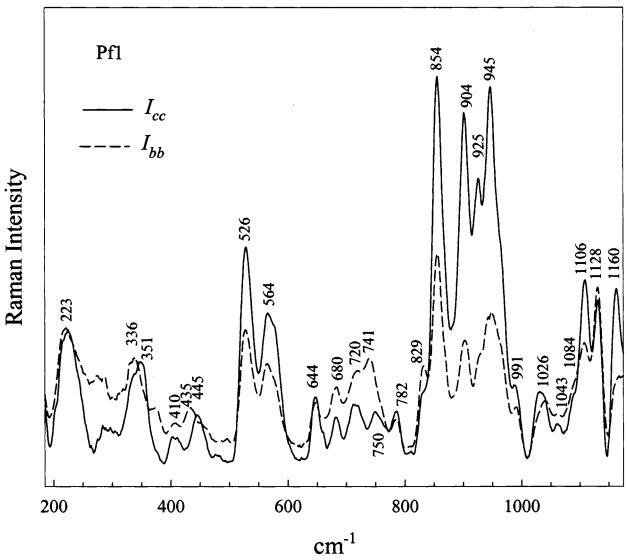

FIGURE 1: Polarized I_{cc} (—) and I_{bb} (---) Raman spectra in the region 200−1170 cm^{-1} obtained with 514.5-nm excitation from an oriented fiber of the Pf1 filamentous virus.

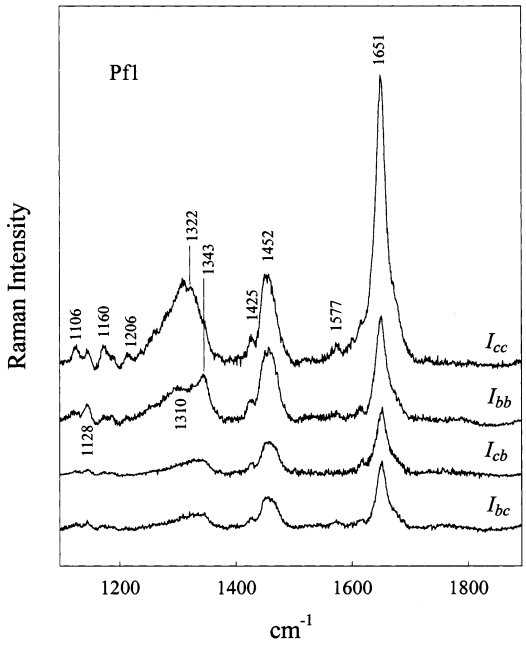

FIGURE 2: From top to bottom: Polarized I_{cc}, I_{bb}, I_{cb}, and I_{bc} Raman spectra in the region 1200−1800 cm^{-1} obtained with 514.5 nm excitation from an oriented fiber of the Pf1 filamentous virus.

Table 1. New insights provided by the presently measured Raman polarizations include the following.

a. Low-Frequency Vibrational Modes of the α*-Helix.* Two Raman bands observed near 336 and 351 cm^{-1} in the unpolarized Raman spectrum of Pf1 have been assigned to main chain vibrations of the subunit α-helix (*7*). Figure 1 demonstrates that in the polarized I_{cc} spectrum the member at 351 cm^{-1} is more intense than that at 336 cm^{-1}, whereas the converse is true in the I_{bb} spectrum. In principle, each main chain vibration of a polypeptide α-helix should consist of two Raman-active components of *A* and E_2 symmetry and two infrared-active components of *A* and E_1 symmetry. Because the subunit α-helix is close to parallel to the *c*-axis, the E_2-type Raman mode is expected to be more intense in the I_{bb} than in the I_{cc} spectrum, whereas the *A*-type Raman mode can be intense in either the I_{cc} or I_{bb} spectrum

Table 1: Raman Polarization, Infrared Dichroism and Vibrational Assignments of Pf1 Virus

Raman[a]			infrared[b]				Raman[a]			infrared[b]			
cm^{-1}	I_{rel}	I_{cc}/I_{bb}	cm^{-1}	A_{rel}	$A_{\parallel}/A_{\perp}$	assignment[c]	cm^{-1}	I_{rel}	I_{cc}/I_{bb}	cm^{-1}	A_{rel}	$A_{\parallel}/A_{\perp}$	assignment[c]
223	3	1.0	–	–	–	u	1084	<1	0.5	–	–	–	R (CN_3 sym str)
336	2	0.2	–	–	–	α-helix (main chain def, E_2)	1106	3	3	–	–	–	A (CH_3 rck)
351	2	>10	–	–	–	α-helix (main chain def, *A*)	1128	3	1.1	–	–	–	side chains (CH_3 rck)
410	1	2	–	–	–	u	1160	3	5	1170	6	0.7	side chains (CH_3 rck)
435	1	<0.1	–	–	–	α-helix (main chain def, E_2)	1206	2	1.6	–	–	–	Y (ring $C^{\beta}-C^{\gamma}$ str)
445	1	>10	–	–	–	α-helix (main chain def, *A*)	–	–	–	1224	4	0.5	DNA bk (PO_2^- asym str)
526	6	1.8	–	–	–	α-helix (amide VI), all side chains	–	–	–	1238	5	0.9	u
564	3	1.9	–	–	–	I, V, L (skl def)	1290	1	–	1292	7	1.5	α-helix (amide III)
644	2	2.0	–	–	–	Y (ring)	1310	5	3	1305	8	–	side chains (CH def)
680	1	1.21	–	–	–	gua (ring)	1322	4	5	–	–	–	α-helix ($C^{\alpha}H$ def, *A*)
720	1	1.2	–	–	–	ade (ring)	1343	4	0.2	–	–	–	α-helix ($C^{\alpha}H$ def, E_2)
741	1	<0.1	–	–	–	α-helix (amide IV)	1387	1	2	1392	1	<1	side chains
750	1	1.2	–	–	–	thy (ring)	1400	<1	2	–	–	–	D, E, C-terminus (CO_2^- str)
782	1	1.22	–	–	–	cyt (ring)	1425	2	2	1420	<1	0.5	side chains, DNA (CH def)
804	<1	2	–	–	–	DNA bk (O−P−O str)	1452	5	1	1454	1	1	side chains (CH_2, CH_3 def)
829	1	0.6	–	–	–	Y (ring, fc)	–	–	–	1518	1	>5	α-helix (amide II, *A*)
854	8	1.8	–	–	–	Y (ring, fc)	–	–	–	1544	5	0.5	α-helix (amide II, E_1)
904	7	2.3	–	–	–	A ($C^{\alpha}-C^{\beta}$ str)	1577	<1	1.5	–	–	–	gua, ade (ring)
925	6	5	–	–	–	V, L (skl str)	1620	<1	0.5	–	–	–	Y (ring)
945	7	1	–	–	–	V, L (skl str)	1651	10	3.0	1651	10	1.25	α-helix (amide I)
991	1	2	–	–	–	u	–	–	–	2963	3	0.8	side chains (al CH str)
1026	1	3	–	–	–	α-helix (main chain str, *A*)	–	–	–	3064	2	3	α-helix (2 × NH def, fc)
1035	1	0.3	–	–	–	α-helix (main chain str, E_2)	–	–	–	3298	10	2	α-helix (NH str)
1043	<1	3	–	–	–	u	–	–	–	3490	3	0.9	side chains, H_2O (OH str)

[a] From data of Figures 1−3 and previous results (*17*). Wavenumbers are accurate to ±1 cm^{-1} for sharp bands and ±3 cm^{-1} for weak bands or shoulders; relative intensities (I_{rel}, arbitrary 0−10 scale) are accurate to ±5% for bands of $I_{rel} > 3$; polarizations (I_{cc}/I_{bb}) are accurate to ±10% unless indicated otherwise in the text. [b] From data of Figures 4 and 5. Wavenumbers are accurate to ±1 cm^{-1} for sharp bands and ±3 cm^{-1} for weak bands or shoulders; relative absorbances (A_{rel}, arbitrary 0−10 scale) are accurate to ±5% for bands of $A_{rel} > 3$; dichroic ratios ($A_{\parallel}/A_{\perp}$) are accurate to ±10% unless indicated otherwise in the text. [c] Abbreviations: al, aliphatic; asym, antisymmetric; bk, backbone; def, deformation; fc, Fermi doublet component; rck, rocking; skl, skeletal; str, stretching; sym, symmetric; u, unknown. Standard one-letter and three-letter abbreviations are given for amino acids and DNA bases, respectively, and standard notation is used for chemical subgroups. Related assignments are given in previous publications (*19*, *33*−*35*, *65*−*68*).

depending upon the form of the vibration. We assign the 351 and 336 cm^{-1} bands to *A* and E_2 modes, respectively, of the α-helix and propose a similar interpretation for the pair of Raman bands observed at 445 (*A* mode) and 435 cm^{-1} (E_2 mode). Both members of the 336/351 cm^{-1} pair and both members of the 435/445 cm^{-1} pair are believed due to skeletal vibrations of the α-helix main chain of the Pf1 subunit. Symmetry splitting of the latter was not resolved in previously reported Raman spectra of Pf1 (*7*).

A main chain vibration of the subunit α-helix may also contribute to the strong Raman band at 526 cm^{-1} (Figure 1), although *A* and E_2 symmetry splitting is not apparent. On the basis of studies of synthetic polypeptides (*44*), the so-called amide VI vibration of the α-helical peptide moiety could occur near 526 cm^{-1}. Such a vibration would involve primarily a bending motion of the carbonyl (C═O) group out of the plane of the peptide (O═C−N−H) moiety, which should give rise to relatively intense Raman scattering. However, the extraordinary intensity of the 526 cm^{-1} band in Pf1 (Figure 1) compared with intensities of similar bands (500−550 cm^{-1} interval) in other filamentous viruses indicates the likelihood of additional underlying Raman bands from side chains present in the Pf1 capsid subunit but absent from other filamentous virus capsid subunits. Likely candidates are certain aliphatic side chains (*7*), as discussed in Section 1c2, below.

The strong Raman band near 564 cm^{-1} (Figure 1) was assigned previously to an amide VI vibration (mainly C═O out-of-plane bending) (*7*). Both the main peak at 564 cm^{-1} and the apparent shoulder at 575 cm^{-1} exhibit $I_{cc} > I_{bb}$, which is not expected if A/E_2 symmetry splitting and the Raman tensor are similar to those of the other low-frequency α-helix modes noted above. Although A/E_2 symmetry splitting could account for the apparent shoulder, a definitive interpretation is not proposed here because the Raman scattering tensor for the amide VI vibration is not known.

In the 680−780 cm^{-1} region of the Raman spectrum, where bands of packaged Pf1 DNA are predominant, an overlapping band assignable to the capsid subunit is observed with prominent I_{bb} intensity at 741 cm^{-1} (Figure 1). Previously, a Raman band at 741 cm^{-1} in the spectrum of the Ff virion was assigned tentatively to the amide IV mode of the subunit main chain (*34*). The amide IV assignment was based in part on the sensitivity of the Ff 741 cm^{-1} band to ^{13}C labeling of the capsid subunit. The 741 cm^{-1} band of Pf1 is similarly proposed as an α-helical amide IV mode. The observation that $I_{bb} > I_{cc}$ supports this assignment because each peptide C═O bond (and therefore each peptide plane) of the Pf1 subunit is directed close to parallel to the virion *c* axis. Thus, the carbonyl in-plane bending vibration should generate the predominant polarizability oscillation along the perpendicular (*b* axis) direction.

b. Amide I, Amide III, and Other Modes of the α*-Helix.* The intense and narrow amide I band at 1651 cm^{-1} (Figure 2) signifies the uniformity of α-helical secondary structure in the Pf1 subunit (*7*, *19*, *43*, *45*). The measured I_{cc}/I_{bb} ratio of 3.0 ± 0.1 is in accord with previous determinations on both Pf1 (*19*) and Ff virions (*25*).

Most filamentous viruses generate characteristically weak Raman amide III bands in the interval 1270−1280 cm^{-1}, as expected for the predominantly α-helical secondary structure (*7*). Still weaker amide III intensity occurs near 1250 cm^{-1}, presumably due to residues at the α-helix ends. Figure 2 suggests that the Raman amide III scattering of the Pf1 subunit is not appreciably polarized, which may reflect a relatively isotropic tensor. The form of the amide III Raman tensor is not presently known.

The peaks at 1322 and 1343 cm^{-1} in the I_{cc} and I_{bb} spectra, respectively, of Figure 2 are also assignable to a main chain vibration of the α-helical capsid subunit. This amide-like vibration involves significant $C^{\alpha}-H$ bond deformation in the $O{=}C-C^{\alpha}-H$ plane coupled with $C-C^{\alpha}$ bond stretching (*46*). Because protein molecules typically contain many CH groups, the $C^{\alpha}-H$ bending vibration has not generally been considered useful for protein structural analysis. Recently, however, we described a method for utilizing the α-helix Raman marker of Pf1 near 1340 cm^{-1} as a source of structural information on the virion assembly (*19*). The present data are consistent with the previous analysis, indicating a low average tilt angle (θ_h) of the subunit α-helix from the virion axis. It is interesting that the *A*-type (1322 cm^{-1}) and E_2-type (1343 cm^{-1}) modes of Pf1 appear at nearly the same wavenumber values as the corresponding *A* and E_2 modes of α-helical poly-γ-benzyl-L-glutamate (PBLG) (*19*). This is noteworthy because the strict α-helical symmetry of PBLG is obviously not sustained for the Pf1 subunit. We note that the nonzero intensities of the 1322 and 1344 cm^{-1} bands in the I_{bb} and I_{cc} spectra, respectively, of Figure 2 confirm that the Pf1 subunit α-helices are not aligned strictly parallel to the *c* axis.

The weak Raman band observed near 1026 cm^{-1} in the I_{cc} spectrum of Figure 1 also appears to exhibit symmetry splitting, by virtue of the shift of the band center to 1035 cm^{-1} in the I_{bb} spectrum. We tentatively assign this band to a main chain vibration of the subunit α-helix, for which the 1026 and 1035 cm^{-1} peaks may correspond to *A* and E_2 components, respectively. In the case of the Ff filamentous virus, a more intense Raman band is observed in this wavenumber region (ca. 1031 cm^{-1}), but exhibits no apparent splitting (*25*) and is confidently assigned to the phenylalanine residues of the Ff subunit (*33*). Because the Pf1 capsid subunit contains no phenylalanine, the polarized Raman spectrum of Pf1 reveals the weak 1026/1035 cm^{-1} couplet of the peptide main chain.

c. Vibrational Modes of the Subunit Side Chains. 1. Tyrosines. The two tyrosine residues (Tyr 25 and Tyr 40) of the Pf1 subunit generate the sharp Raman band that is observed in Figure 1 at 644 cm^{-1}. This band has been assigned to a vibration of the *para*-phenoxyl ring that is probably similar in nature to the mode of benzene occurring at 605 cm^{-1} (*47*, *48*). The Raman tensor of the 644 cm^{-1} band has principal axes *x* and *y* that are rotated by 45° from the line intersecting the C^{γ} and C^{ζ} atoms. The tensor quotients r_1 ($\equiv \alpha_{xx}/\alpha_{zz}$) and r_2 ($\equiv \alpha_{yy}/\alpha_{zz}$) have values of 6.9 and −5.9, respectively (*49*). The large tensor ratios and significant polarization observed for this band ($I_{cc}/I_{bb} = 2.0$) are favorable to gaining information about the average phenoxyl ring orientation for Tyr 25 and Tyr 40. (See Discussion Section, below.)

The strong Raman band at 854 cm^{-1} (Figure 1) is well established as being due to the phenoxyl ring breathing vibration of Pf1 tyrosines (*7*, *36*). The Raman tensor is known to be relatively isotropic with respect to the in-plane components ($\alpha_{xx} \approx \alpha_{yy}$), but the out-of-plane component α_{zz} differs greatly from α_{xx} or α_{yy} (*49*). Accordingly, the large polarization observed provides strong evidence that the phenoxyl ring planes of Tyr 25 and Tyr 40 cannot both be perpendicular to the virion axis. (See below.)

The weak but well-resolved Raman band at 1206 cm^{-1} in Figure 1 is also assignable to Pf1 tyrosines. In the spectrum of the L-tyrosine crystal, the corresponding band, which occurs at 1200 cm^{-1}, has been assigned to a vibration involving predominantly the stretching of the $C^{\beta}-C^{\gamma}$ bond (*49*). Ab initio calculation determines the wavenumber value for this mode to be 1209 cm^{-1} and predicts that the polarizability oscillation is greatest along the $C^{\beta}-C^{\gamma}$ bond. Experimental data obtained on an oriented L-tyrosine single crystal indicate that the polarized Raman spectrum (I_{bb}) is most intense when the crystallographic *b*-axis is parallel to the $C^{\beta}-C^{\gamma}$ bond, consistent with the ab initio calculation (*49*). For the 1206 cm^{-1} band of Pf1, the observation that I_{cc} is greater than I_{bb} (Figure 1) implies that the average Pf1 tyrosyl $C^{\beta}-C^{\gamma}$ bond direction is parallel to the virion axis.

2. Alanines and Other Aliphatic Side Chains. The strong Raman band at 904 cm^{-1} (Figure 1) has been assigned to alanyl $C^{\alpha}-C^{\beta}$ bond stretching (*7*, *32*). The band exhibits significant polarization ($I_{cc}/I_{bb} \approx 3$). The greatest polarizability oscillation for this vibration is expected to be along the direction of the $C^{\alpha}-C^{\beta}$ bond. We may therefore conclude that most or all of the seven alanine side chains per subunit are oriented with respect to the virion axis so that the $C^{\alpha}-C^{\beta}$ bonds are inclined at an angle that is appreciably smaller than 54.7°.

Other subunit side chains present in relatively large numbers, such as Ile (*6*), Val (*5*) and Leu (*4*), are expected to contribute to the Pf1 Raman spectrum. The two strong bands at 526 and 564 cm^{-1} are considered to be mostly due to skeletal deformation vibrations of Ile, Val, and Leu, although the main chain α-helix may also contribute, as noted above. In Pf1 the 526 cm^{-1} band is stronger than the 564 cm^{-1} band, and the Raman scattering is anisotropic ($I_{cc} > I_{bb}$). In Ff, on the other hand, the corresponding bands are of nearly equal intensity and the lower wavenumber component (533 cm^{-1}) exhibits isotropic scattering (*7*, *35*). Such spectral differences between Pf1 and Ff may reflect not only the fact that the total of Ile, Val, and Leu residues per subunit is quite different but also that the average orientations of the side chains may differ in the two virion assemblies. The intense 945 cm^{-1} Raman band of Pf1, which has been assigned to vibrations of Val and Leu side chains (*7*, *35*), is likewise appreciably more intense than its counterpart in Ff (936 cm^{-1}) (*7*). Again, this may reflect the greater number of methyl-containing side chains in Pf1 (18) than in Ff (*12*).

The Raman spectral interval 1100−1160 cm^{-1} is expected to contain bands due to rocking vibrations of the CH_3 groups of Ala, Val, Leu, and Ile (*7*, *32*, *35*). In Ff, CH_3 rocking modes of aliphatic side chains have been assigned to bands at 1107 cm^{-1} (Ala), 1130 cm^{-1} (Ile, Val, Leu), and 1158 cm^{-1} (Ile, Val) (*7*). Accordingly, the CH_3 modes of Pf1 may be assigned to Raman bands at 1106 cm^{-1} (Ala), 1128 cm^{-1} (Ile, Val, Leu), and 1160 cm^{-1} (Ile, Val). We note that the

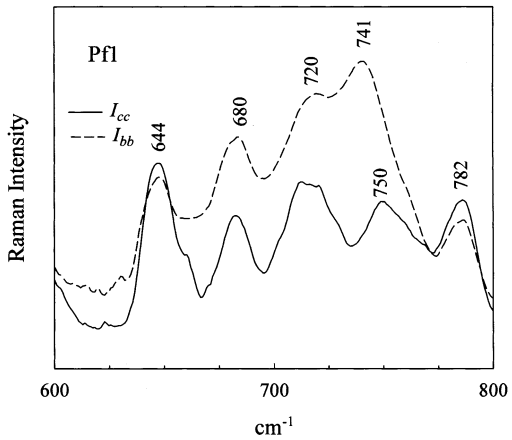

FIGURE 3: Expansion of the polarized I_{cc} (—) and I_{bb} (---) Raman spectra of Figure 1 in the region 600−800 cm^{-1}.

intensity ratio of the Pf1 bands at 1128 and 1106 cm^{-1} (Figure 1) is greater than the intensity ratio of the Ff bands at 1130 and 1107 cm^{-1} (*7*), which is consistent with the respective subunit amino acid compositions of Pf1 [(Ile + Val + Leu)/(Ala) = 15/7] and Ff [(Ile + Val + Leu)/(Ala) = 10/10] (*1*). The Raman polarizations are also significantly different. Thus, for the 1128 cm^{-1} band of Pf1, $I_{bb} = I_{cc}$ (Figure 1), whereas for the 1130 cm^{-1} band of Ff, $I_{cc} \ll I_{bb}$ (*25*). This signifies a greater tilt from the virion axis for the average C−CH_3 bond of the Ile and Val residues in Pf1 subunits than in those of Ff.

3. Arginine. At present, definitive vibrational assignments for the arginyl side chain in proteins have not been developed. However, preliminary studies of arginine model compounds, including methyl guanidine, poly-L-arginine and isotopic variants of L-arginine, suggest possible Raman assignments for the terminal guanidinium group of the arginyl side chain (K. Nakamura, P. Bondre, M. Tsuboi, and G. J. Thomas, Jr., 2002, unpublished results.) Prominent among these is a Raman band near 1080−1090 cm^{-1}. Interestingly, the Raman spectrum of Pf1 contains a weak band at 1084 cm^{-1} (Figure 1), which could arise in part from the Arg 44 side chain of the capsid subunit. Packaged ssDNA is also expected to contribute weak Raman intensity near 1090 cm^{-1} from the PO_2^- symmetric stretching mode. However, the weak Raman band at 1084 cm^{-1} is not likely to be caused by DNA phosphates because it becomes vanishingly weak in D_2O solutions, exhibits prominent anisotropy ($I_{cc} < I_{bb}$), and has no counterpart in Ff. Accordingly, we tentatively assign the Arg 44 side chain of the Pf1 subunit as the main contributor to the Raman marker at 1084 cm^{-1}. This assignment—specifically, to a skeletal in-plane NC_3 stretching mode of the guanidinium moiety—accounts for the specificity, polarization and deuteration properties of the 1084 cm^{-1} marker. Importantly, the polarization implies that the direction of the $C^{\delta}-N^{\epsilon}$ bond is likely to be perpendicular to the *c* axis.

d. Vibrational Modes of the Packaged ssDNA Genome. Raman bands of the deoxynucleosides of packaged Pf1 DNA occur at 680 (dG), 720 (dA), 750 (dT), and 782 cm^{-1} (dC) (Figure 3). Each band corresponds to a relatively symmetrical stretching vibration ("ring breathing") of the six-membered ring of the base (*50*), and each is diagnostic of the sugar pucker and glycosyl orientation of the attached deoxyribosyl moiety (*51*−*55*). The DNA Raman markers in the interval

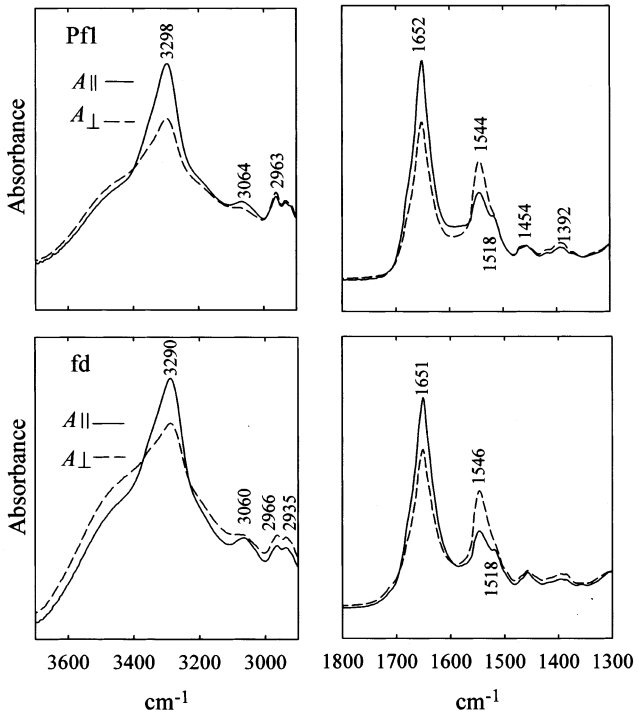

FIGURE 4: Dichroic $A_{\|}$ (—) and $A_{\perp}$ (---) infrared absorption spectra of the filamentous viruses Pf1 (top panels) and Ff (bottom panels) in the regions 3700−2900 cm^{-1} (left panels) and 1800−1300 cm^{-1} (right panels).

600−800 cm^{-1} of Figure 3 indicate the C2′-endo/anti conformation for deoxynucleosides of the packaged genome, in accordance with previously reported unpolarized Raman results (*10*, *17*). The polarized Raman data of Figure 3 also establish the position of the dT marker more accurately (750 cm^{-1}) than previously (746 cm^{-1})(*7*)), despite overlap with a more intense band near 741 cm^{-1} that evidently arises from the capsid subunit. The 750 cm^{-1} dT marker clearly identifies the C2′-endo/anti conformation for dT (*56*). It is interesting that all DNA marker bands of Figure 3 exhibit $I_{cc} \neq I_{bb}$, demonstrating that the DNA bases cannot be randomly oriented within the capsid.

A Raman difference spectrum computed between the two traces of Figure 3 ($I_{bb} - I_{cc}$, data not shown) suggests that the I_{bb} spectrum contains broad underlying features between 650 and 775 cm^{-1} in addition to a fairly sharp band near 741 cm^{-1} that is not apparent in the I_{cc} spectrum. The broad I_{bb} features are also observed in polarized Raman spectra of the Ff filamentous virus (*25*), suggesting a common origin, possibly from polarized Raman scattering of H_2O in the hydrated fiber.

2. Infrared Bands of Pf1. Polarized infrared spectra of the oriented Pf1 virus and parallel ($A_{\|}$) and perpendicular ($A_{\perp}$) infrared absorption intensities are compared with corresponding data for oriented Ff in Figure 4 (3700−2900 and 1800−1300 cm^{-1}) and Figure 5 (1350−1150 cm^{-1}). In accordance with IUPAC guidelines, all infrared spectra are illustrated here with the wavenumber axis increasing from right to left. We note that these polarized infrared spectra reflect substantial improvements over previously reported data (*9*, *31*), with regard to spectral resolution, signal intensity and degree of sample orientation. The data of Figures 4 and 5 show that the dichroic ratios ($D = A_{\|}/A_{\perp}$) of most infrared bands of both viruses are very different from unity. This confirms

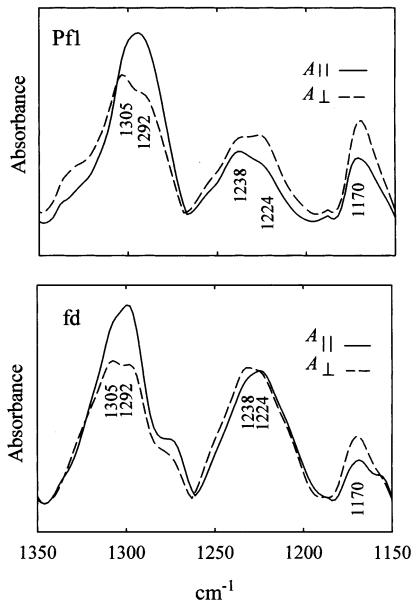

FIGURE 5: Dichroic $A_{\|}$ (—) and $A_{\perp}$ (---) infrared absorption spectra of the filamentous viruses Pf1 (top panel) and Ff (bottom panel) in the region 1350−1150 cm^{-1}.

that the virions are ordered nonrandomly and that various molecular subgroups of the virions are specifically oriented within the virion. Nevertheless, the degree of virion alignment in the oriented films prepared for infrared spectroscopy is not as high as that achieved in the oriented fibers prepared for Raman spectroscopy, as judged by birefringence observed in a light microscope. A quantitative assessment of virion disorder in the films is given below. The infrared data are compiled with the Raman data in Table 1.

a. Vibrational Modes of the Capsid Subunit. The strong Pf1 band at 3298 cm^{-1} (Figure 4, upper left panel) is assigned to N−H bond stretching of the subunit peptide groups. The position of this N−H stretching mode is as expected for strong N−H···O hydrogen bonds in the subunit α-helix. Because the band represents a virtually pure N−H bond stretch, the transition dipole moment should lie essentially along the bond direction. Thus, the observation of a dichroic ratio greater than unity ($D_{3298} = 2$, i.e., parallel dichroism) is consistent with the expectation that N−H···O hydrogen bonds of the subunits are aligned close to parallel to the *c* axis. Not surprisingly, the corresponding infrared band of Ff also exhibits similar parallel dichroism ($D_{3290} = 2$). These results are consistent with the low tilt angles ($\theta_h \sim 16°$) determined for the subunit α-helices in both class I and class II virion assemblies (*19*, *25*).

The strong Pf1 band at 1652 cm^{-1} (Figure 4, upper right panel) is assignable to the infrared amide I mode of the subunit α-helix, in agreement with the Raman amide I counterpart (Figure 2). The infrared transition dipole moment for amide I is inclined from the α-helix axis by about 29° (*19*, *57*), which accounts for the observed parallel dichroism of Pf1 ($D_{1652} = 1.4$) and Ff ($D_{1651} = 1.4$).

Pf1 and Ff are also expected to exhibit a prominent infrared amide II band. For both viruses, we observe an intense infrared amide II band at 1545 ± 1 cm^{-1} (Figure 4, right panels), which exhibits a dichroic ratio less than unity, i.e., perpendicular dichroism ($D_{1545} = 0.5$). This is assigned to the α-helix E_1-type component of amide II, which is expected to occur near 1555−1545 cm^{-1} with $D < 1.0$. The weak shoulder to the 1545 cm^{-1} band that is observed near 1518 cm^{-1} in both Pf1 and Ff is assigned to an amide II *A*-type mode, which is expected to exhibit much lower intensity than the E_1 mode (*41*, *57*, *58*). The perpendicular dichroism of amide II is also consistent with low α-helix tilt angle.

Pf1 has an intense infrared band at 1238 cm^{-1} (Figure 5), which exhibits perpendicular dichroism. Although a definitive assignment cannot be made at present, the high intensity of the band, as well as the occurrence of a similarly dichroic counterpart in Ff, suggests a main chain mode of the capsid subunit, possibly amide III. Because high infrared intensity is not expected for amide III, the band could also be due to a side chain such as tyrosine that is common to both Pf1 and Ff subunits.

b. Vibrational Modes of the Packaged ssDNA Genome. Pf1 exhibits a prominent infrared band near 1224 cm^{-1} (Figure 5), which is confidently assigned to phosphodioxy (PO_2^-) groups of the packaged ssDNA molecule. The band is due to the antisymmetric PO_2^- stretching vibration. The transition dipole moment of this vibration must be directed along the line connecting the two oxygen atoms (O···O). The 1224 cm^{-1} band clearly exhibits perpendicular dichroism in Pf1, which indicates that the O···O line of the average phosphate of packaged Pf1 DNA is close to perpendicular to the virion axis. This finding indicates that the DNA phosphates are specifically ordered with respect to the capsid subunits (*3*).

The intensity of the 1224 cm^{-1} band of Ff is considerably greater than that of Pf1, consistent with the fact that the ssDNA genome of Ff constitutes a much greater percentage of the virion mass (∼14% in Ff vs ∼6% in Pf1). Interestingly, the 1224 cm^{-1} band of Ff exhibits no dichroism (Figure 5). This indicates that phosphates of the packaged Ff DNA genome, unlike those of Pf1, are arranged either randomly or at the magic angle of 54.7°.

DISCUSSION

Orientation of the Subunit α-Helix with Respect to the Virion Axis. The present data provide two independent means of determining the subunit α-helix tilt angle (θ_h) of Pf1. First, the polarized Raman amide I intensity ratio, $I_{cc}/I_{bb} = 3.0 \pm 0.1$, may be inserted into eq 1 to solve for θ_h (*25*)

$$I_{cc}/I_{bb} = (4)(0.537 \sin^2\theta_h + \cos^2\theta_h)^2/(0.537 \cos^2\theta_h + \sin^2\theta_h + 0.537)^2 \quad (1)$$

This yields $\theta_h = 16° \pm 4°$. Here the uncertainty indicates the range of values obtained in repeated independent measurements. Second, the polarized Raman band profiles of Pf1 in the 1320−1350 cm-1 region provide $\theta_h = 20° \pm 10°$ (*19*), in agreement with the Raman amide I determination. The results indicate that the subunit tilt angle in Pf1 is the same as that in Ff. We conclude that despite dissimilar arrangements of subunits in virions of class II and class I symmetries, the subunit tilt angles are similar.

Orientations of Tyrosine Side Chains (Tyr 25 and Tyr 40). The two tyrosines per Pf1 subunit (Tyr 25, Tyr 40) yield prominent and highly polarized Raman bands at 644 cm^{-1} ($I_{cc}/I_{bb} = 2.0$), 854 cm^{-1} ($I_{cc}/I_{bb} = 1.8$) and 1206 cm^{-1}

Table 2: Raman Tensors of the Tyrosine Side Chain[a]

Raman band (cm^{-1})	Raman tensor principal axes	Raman tensor ratios[b]
642	x (45° from $C^{\gamma}\cdots C^{\zeta}$ line)	$r_1 = 6.93$
	y ($\perp$ to x, in ring plane)	$r_2 = -5.87$
	z ($\perp$ to ring plane)	
829	x (along $C^{\gamma}\cdots C^{\zeta}$ line)	$r_1 = 2.2$
	y ($\perp$ to x, in ring plane)	$r_2 = 2.0$
	z ($\perp$ to ring plane)	
1206	x (along $C^{\gamma}\cdots C^{\zeta}$ line)	$r_1 = 1.43$
	y ($\perp$ to x, in ring plane)	$r_2 = 0.54$
	z ($\perp$ to ring plane)	

[a] Determined from a polarized Raman analysis of an oriented single crystal of L-tyrosine (*49*). [b] $r_1 = \alpha_{xx}/\alpha_{zz}$, $r_2 = \alpha_{yy}/\alpha_{zz}$.

($I_{cc}/I_{bb} = 1.6$). Assuming that the Raman tensors for these three bands are the same as those determined previously for the corresponding Raman bands in the single crystal of L-tyrosine (*49*), the polarized Raman measurements on Pf1 may be exploited to obtain information about the tyrosine side chain orientations as follows.

The phenolic ring orientation is described in terms of two Eulerian angles, θ and χ, which relate the virion coordinate system (*abc*) to the Raman tensor coordinate system (*xyz*) of a given vibrational mode. The *abc* system is fixed to the virion, with *c* as the virion axis, whereas *a* and *b* are equivalent and perpendicular to *c*. θ is the angle between the *z* and *c* axes, while χ is the angle between *y* and the line of intersection of the *xy* and *ab* planes (*28*). The Raman tensor coordinate systems for the 854 and 1206 cm^{-1} modes are the same, viz. *x* is parallel to the line connecting C^{γ} and C^{ζ}, *y* is perpendicular to *x* in the plane of the phenolic ring and bisects the $C^{\delta 1}-C^{\epsilon 1}$ and $C^{\delta 2}-C^{\epsilon 2}$ bonds, and *z* is perpendicular to the phenolic ring plane. The Raman tensor coordinate system for the 644 cm^{-1} band is not the same as those for the 854 or 1206 cm^{-1} bands, but can be generated from the latter by a 45° rotation about *z* (Table 2) (*28*, *49*).

The polarized Raman intensity ratio I_{cc}/I_{bb} is given in terms of θ and χ by eq 2 (*59*):

$$I_{cc}/I_{bb} = 4[\sin^2\theta\,(r_1\cos^2\chi + r_2\sin^2\chi) + \cos^2\theta]^2/ [\cos^2\theta\,(r_1\cos^2\chi + r_2\sin^2\chi) + r_1\sin^2\chi + r_2\cos^2\chi + \sin^2\theta]^2 \quad (2)$$

For the 854 cm^{-1} band, using $I_{cc}/I_{bb} = 1.8$ and the known r_1 and r_2 values (Table 2), we obtain a contour line in (θ,χ) space as shown in Figure 6. Similarly, Figure 6 shows the contour line obtained for the 1206 cm^{-1} band ($I_{cc}/I_{bb} = 1.6$, with r_1 and r_2 values also as given in Table 2). Finally, the corresponding data for the 644 cm^{-1} band ($I_{cc}/I_{bb} = 2.0$, with r_1 and r_2 given in Table 2) yield the contour line that is plotted on the same (θ,χ) coordinate system of Figure 6, after accounting for the required 45° rotation about *z*. The intersection of the three contour lines represents the region of (θ,χ) space that corresponds to the average phenolic ring orientation of Tyr 25 and Tyr 40, i.e., $\theta = 76 \pm 10°$ and $\chi = 34 \pm 10°$. Here, the uncertainties reflect the estimated error limits in the I_{cc}/I_{bb} measurements (Figures 1 and 2), which are much larger than error limits in the Raman tensor determinations (Table 2).

For comparison with the experimental results, we include in Figure 6 the Eulerian angles predicted for Tyr 25 and Tyr 40 in the molecular models proposed for the Pf1 capsid by Liu and Day (*16*) (Protein Data Bank entry 1PF1) and Marvin and co-workers (*3*, *60*, *61*) (Protein Data Bank entry 2IFN). Both models project values for θ that are between 68° and 85° for each tyrosine, which is consistent with our experimental result (average $\theta = 76 \pm 10°$). A value for θ close to 90° corresponds to a phenolic ring plane that is close to parallel to the virion axis. With regard to χ, only the 1PF1 model projects a value ($\chi \sim 31°$ for Tyr 25) that is close to the experimental average (34° ± 10°). Otherwise the 1PF1 and 2IFN models differ significantly from one another and from the experimental determination, as seen in Figure 6. We note that a value for χ close to 30−35° implies that the $C^{\zeta}-O^{\eta}$ bond of the phenoxyl moiety is inclined at a low angle from the virion axis, as shown for Tyr 25 of the 1PF1 model in Figure 7.

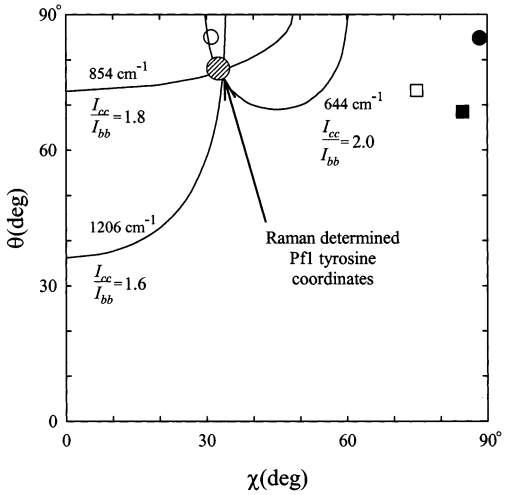

FIGURE 6: Contour plots in (θ,χ) space of the polarized Raman intensity ratios I_{cc}/I_{bb} of the tyrosine marker bands at 644, 854, and 1206 cm^{-1} in the spectrum of the Pf1 virus. The plots were obtained from eq 2 using the measured I_{cc}/I_{bb} values for the data of Figures 1 and 2 and the known r_1 and r_2 values of Table 2. The point of intersection of the three plots gives the average Pf1 tyrosine coordinates ($\theta = 76° \pm 10°$, $\chi = 34° \pm 10°$). These are designated by the hatched circle, the area of which reflects the experimental errors of polarized Raman measurements (*24*, *28*). Also shown are the θ,χ coordinates predicted by the Pf1 molecular models of Liu and Day (○ Tyr 25, ● Tyr 40; Protein Data Bank entry 1PFN) (*16*) and Marvin and co-workers (□ Tyr 25, ■ Tyr 40; Protein Data Bank entry 2IFN) (*61*).

The presently determined coordinates for the phenolic moieties of Tyr 25 and Tyr 40, revised from those of the 1PF1 model (*16*) in accordance with Figure 6, are listed in Table 3. It must be emphasized that the present experimental determination of tyrosine side chain orientations in Pf1 is based upon the assumption that the Tyr 25 and Tyr 40 residues of the capsid subunit contribute equally to the observed polarized Raman intensity ratios (I_{cc}/I_{bb}). In previous determinations of the orientations of the two tyrosine side chains (Tyr 21 and Tyr 24) per subunit of the class I Ff virion, the separate spectral contributions of Tyr 21 and Tyr 24 could be demonstrated as equal by examining site-specific mutants (Y21M and Y24M) in addition to the wild-type virus (*27*, *28*). Unfortunately, tyrosine mutant variants of Pf1 are not sufficiently viable to permit isolation for spectroscopic analysis. Nevertheless, it is interesting to note that the two tyrosines of the Ff subunit exhibit orientations that are nearly identical to one another, viz. $\theta \sim 70°$ and $\chi \sim 36°$.

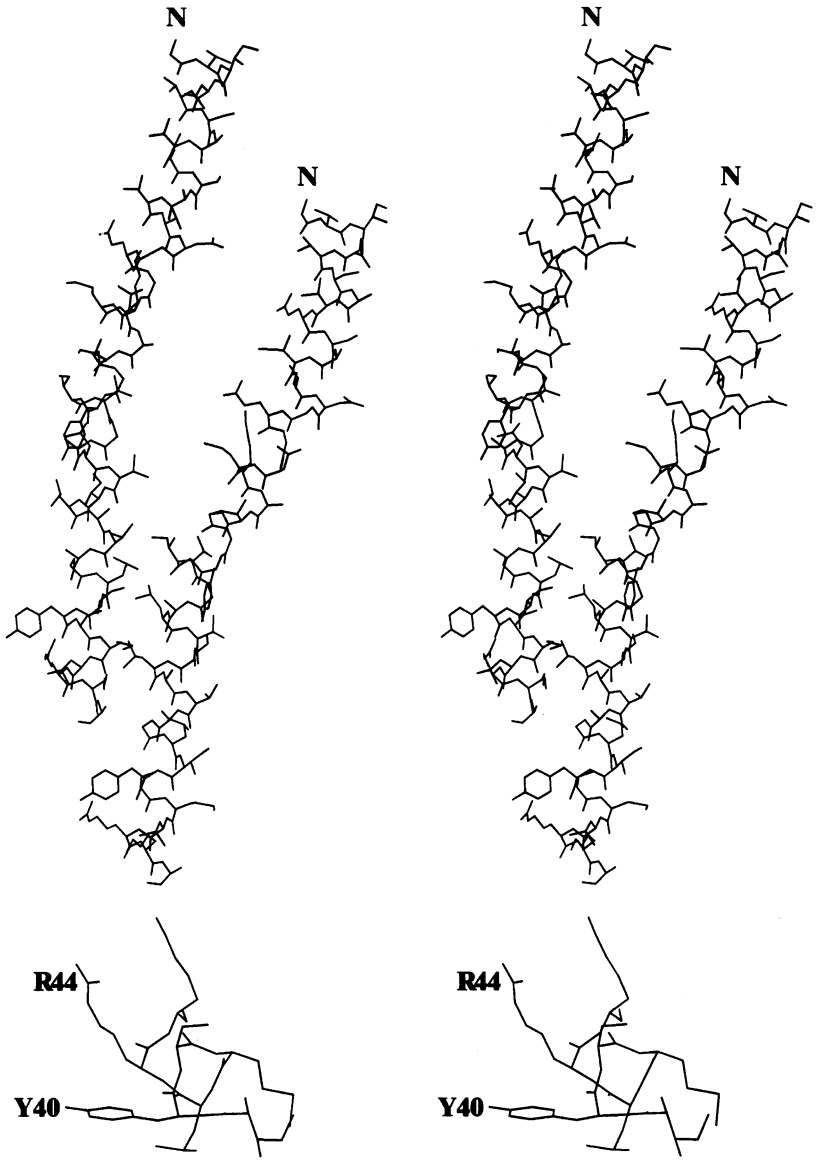

FIGURE 7: (top) Stereo representation of two neighboring subunits ($k = 0$ and $k = 5$) of the Pf1 capsid. The model incorporates atomic coordinates of the Tyr 40 phenoxyl ring (Table 3) determined from the polarized Raman analysis of Figure 6. Other atomic coordinates are from Protein Data Bank entry 1PFN (*16*). (bottom) Stereo representation of the C-terminal segment of the capsid subunit showing residues Tyr 40 and Arg 44.

Table 3: Proposed Atomic Coordinates for the Phenoxyl Ring of Tyr 40

atom (*N*)	x	y	z
C^{β} (547)	2.611	−14.269	5.552
C^{γ} (548)	1.324	−14.096	4.737
$C^{\delta 1}$ (549)	1.378	−13.868	3.358
$C^{\delta 2}$ (550)	0.083	−14.176	5.377
$C^{\epsilon 1}$ (551)	0.199	−13.728	2.627
$C^{\epsilon 2}$ (552)	−1.092	−14.033	4.644
C^{ζ} (553)	−1.033	−13.810	3.271
O^{η} (554)	−2.183	−13.674	2.551

[a] Obtained by revising the previously proposed coordinates of Liu and Day (*16*) in accordance with the polarized Raman results (rotation of −64° about the $C^{\alpha}-C^{\beta}$ bond and a rotation of +56° about the $C^{\beta}-C^{\gamma}$ bond).

Remarkably, these separately determined (θ,χ) coordinates for Tyr 21 and Tyr 24 of Ff are also very close to the average (θ,χ) coordinates of Tyr 25 and Tyr 40 of Pf1. Evidently, a tyrosine side-chain orientation in which both the phenoxyl ring plane and the phenolic $C^{\zeta}-O^{\eta}$ bond are relatively close to parallel to the fiber axis is favored for α-helical subunits of filamentous virus capsids. The close correspondence between the previously determined Tyr 21 and Tyr 24 orientations in Ff (*27*, *28*) and presently determined average tyrosine orientations in Pf1 lends confidence to the validity of the assumption that Tyr 25 and Tyr 40 are oriented similarly.

A further limitation of the present determination is ambiguity in the polarity of each Raman tensor coordinate system (*xyz*). Because eq 2 is quadratic in r_1 and r_2, the signs of the Raman tensor components and consequently the absolute directionalities of the residue orientations are lost. Thus, while the inclinations of the phenoxyl ring plane and $C^{\zeta}-O^{\eta}$ bond are established in relation to the virion axis (Figure 7), it is not known whether the $C^{\zeta}-O^{\eta}$ line points to the head or tail of the virion.

Orientations of DNA Phosphates. The infrared band at 1224 cm^{-1}, which is assigned to the antisymmetric stretching vibration of the phosphodioxy group, exhibits dichroism that

is potentially informative of the average phosphate group orientation. If we define ϕ as the angle of inclination between the virion axis and the line connecting the nonesterified phosphate oxygens (O···O line), the dichroic ratio of the 1224 cm^{-1} band is related to ϕ by eq 3:

$$D = A_{\parallel}/A_{\perp} = 2(\cos^2 \phi + g)/(\sin^2\phi + 2g) \qquad (3)$$

The parameter g, which indicates the degree of imperfection in virion alignment in the sample film, is zero for perfect molecular orientation and infinity for completely random molecular orientation. For a given film, g is evaluated by measuring D for a band of known dichroic ratio. Here, we employ the 1544 cm^{-1} band for which $D = 0.45$ (Figure 4). The 1544 cm^{-1} band is the amide II collective mode of E_1-type symmetry and should have no absorption component parallel to the subunit α-helix axis. Because $\phi = \theta_h = 16°$, eq 3 yields $g = 0.24$. Substitution of $g = 0.24$ and the measured dichroic ratio $D = 0.50 \pm 0.05$ (Figure 5) into eq 3 yields $\phi = 71° \pm 10°$ as the angle of inclination of the phosphodioxy O···O line from the virion axis. This inclination angle is lower than the value of ∼90° estimated previously on the basis of solid-state NMR ^{31}P chemical shift data (*62*). However, it is within experimental uncertainty of the value (61°) proposed on the basis of symmetry arguments for phosphates of the packaged DNA in the 1PF1 model (*16*). Thus, the polarized infrared results, like the polarized Raman results noted above, provide experimental support for the 1PF1 model.

Orientations of DNA Base Residues. Raman polarizations of the DNA base marker bands in the region 650−800 cm^{-1} (Figures 2 and 3 and Table 1) contain information about the orientations of the bases with respect to the virion axis. Each base marker exhibits $I_{cc}/I_{bb} \neq 1$, indicating in each case a nonrandom base orientation. However, more detailed knowledge of the Eulerian parameters (θ,χ) for any base would require reliable I_{cc}/I_{bb} measurements on additional base marker bands of known Raman tensor characteristics. Unfortunately, such information is not presently available, owing to the overlap of other base markers either with one another or with bands due to the capsid subunits. Despite this paucity of data, it is interesting to compare the available results with base orientations proposed by Liu and Day for the packaged ssDNA genome of the 1PF1 model (*16*). For this purpose, we consider the cytosine marker at 782 cm^{-1} (Figure 3), for which the Raman tensor can be transferred from a polarized Raman study of the cytidine crystal (*63*). Using this tensor ($r_1 = 3.8$ and $r_2 = 3.2$, where the x, y and z principal axes are, respectively, along the C5═C6 bond, along the N6···C5 line and perpendicular to the base plane), the cytosine marker at 782 cm^{-1} is calculated according to the geometry of the 1PF1 model to have a polarized Raman intensity ratio $I_{cc}/I_{bb} = 1.22$. This compares favorably with the measured value of 1.25 ± 0.05 (Figure 3). Thus, the base orientation proposed by Liu and Day (*16*) is also consistent with the polarized Raman data.

CONCLUDING SUMMARY

In previous applications of methods of polarized vibrational spectroscopy (Raman, UVRR and infrared) to filamentous viruses, the subunit orientations and the aromatic side chain conformations were determined. In the case of Ff, which has been studied most extensively, the Tyr 21, Tyr 24, and Trp 26 side-chain conformations were independently resolved (*24*, *26*−*28*). The average angle of inclination of the Ff subunit α-helix from the virion axis was also determined ($\theta_h = 16° \pm 4°$) (*25*).

In the case of Pf1, we previously proposed a novel polarized Raman method based upon the assignment of a key α-helix marker near 1340−1345 cm^{-1} to determine θ_h (*19*). This application yielded an approximate helix inclination angle of $\theta_h = 20° \pm 10°$ for the Pf1 subunit. In the present work we have used both polarized Raman and polarized FTIR measurements of amide I, amide II and amide III bands to confirm and refine θ_h to $16° \pm 4°$ for the Pf1 subunit, a value that is indistinguishable from the θ_h determined for the Ff subunit. The present study also establishes that the average phenolic side chain orientation of the Pf1 tyrosines (Tyr 25, Tyr 40) is the same as that of the Ff tyrosines (Tyr 21, Tyr 24). Thus, despite major differences between Pf1 and Ff in capsid symmetry, subunit amino acid sequences and intersubunit contacts, the α-helices are similarly inclined and the tyrosines are similarly oriented with respect to the virion axis.

The present investigation also reveals that the nucleotides of the packaged Pf1 DNA genome are not randomly oriented with respect to the virion axis. DNA phosphates are positioned so that the O···O line of the phosphodioxy group oxygens intersects the virus axis at 71°. In addition the deoxynucleosides of Pf1 uniformly adopt the C2′-endo/anti conformation and the base residues are nonrandomly oriented with respect to the virion axis. We interpret the structural details of Pf1 that are revealed by the polarized Raman and FTIR measurements as largely supportive of the molecular model proposed by Liu and Day (*15*, *16*).

Finally, we note that the Raman and infrared results on Pf1 suggest a number of new vibrational assignments for the capsid subunits (Table 1). Of particular interest is the Raman marker of the arginyl guanidinium moiety at 1084 cm^{-1}. Further study of model compounds will be required to confirm this assignment. If confirmed and augmented with Raman tensor determinations, refined polarization measurements could serve as a basis for evaluating the orientation of the guanidinium moiety with respect to Tyr 40 and the prospect of cation−π interaction between the Arg 44 and Tyr 40 side chains. Cation−π interaction between an arginine (Arg 37) and a tryptophan (Trp 38) side chain is supported by experimental results recently obtained on the class II filamentous virus Pf3 (*64*, *65*).

REFERENCES

1. Day, L. A., Marzec, C. J., Reisberg, S. A., and Casadevall, A. (1988) *Annu. Rev. Biophys. Biophys. Chem. 17*, 509−539.
2. Welsh, L. C., Symmons, M. F., and Marvin, D. A. (2000) *Acta Crystallogr., Sect. D: Biol. Crystallogr. 56* (Pt. 2), 137−150.
3. Welsh, L. C., Marvin, D. A., and Perham, R. N. (1998) *J. Mol. Biol. 284*, 1265−1271.
4. Zweckstetter, M., and Bax, A. (2001) *J. Biomol. NMR 20*, 365−377.
5. Zweckstetter, M., and Bax, A. (2001) *J. Am. Chem. Soc. 123*, 9490−9491.
6. Torbet, J., and Maret, G. (1979) *J. Mol. Biol. 134*, 843−845.
7. Thomas, G. J., Jr., Prescott, B., and Day, L. A. (1983) *J. Mol. Biol. 165*, 321−356.
8. Cross, T. A., Tsang, P., and Opella, S. J. (1983) *Biochemistry 22*, 721−726.

9. Fritzsche, H., Tsang, P., Opella, S. J., and Kallenbach, N. R. (1986) *Stud. Biophys. 116*, 175−180.
10. Thomas, G. J., Jr., Prescott, B., Opella, S. J., and Day, L. A. (1988) *Biochemistry 27*, 4350−4357.
11. Day, L. A., Casadevall, A., Prescott, B., and Thomas, G. J., Jr. (1988) *Biochemistry 27*, 706−711.
12. Nambudripad, R., Stark, W., and Makowski, L. (1991) *J. Mol. Biol. 220*, 359−379.
13. Nambudripad, R., Stark, W., Opella, S. J., and Makowski, L. (1991) *Science 252*, 1305−1308.
14. Clack, B. A., and Gray, D. M. (1992) *Biopolymers 32*, 795−810.
15. Kostrikis, L. G., Liu, D. J., and Day, L. A. (1994) *Biochemistry 33*, 1694−1703.
16. Liu, D. J., and Day, L. A. (1994) *Science 265*, 671−674.
17. Wen, Z. Q., Armstrong, A., and Thomas, G. J., Jr. (1999) *Biochemistry 38*, 3148−3156.
18. Blanch, E. W., Bell, A. F., Hecht, L., Day, L. A., and Barron, L. D. (1999) *J. Mol. Biol. 290*, 1−7.
19. Tsuboi, M., Suzuki, M., Overman, S. A., and Thomas, G. J., Jr. (2000) *Biochemistry 39*, 2677−2684.
20. Day, L. A., Wiseman, R. L., and Marzec, C. J. (1979) *Nucleic Acids Res. 7*, 1393−1403.
21. Marzec, C. J., and Day, L. A. (1983) *Biophys. J. 42*, 171−180.
22. Allemand, J. F., Bensimon, D., Lavery, R., and Croquette, V. (1998) *Proc. Natl. Acad. Sci. U.S.A. 95*, 14152−14157.
23. Bustamante, C., Smith, S. B., Liphardt, J., and Smith, D. (2000) *Curr. Opin. Struct. Biol. 10*, 279−285.
24. Tsuboi, M., Overman, S. A., and Thomas, G. J., Jr. (1996) *Biochemistry 35*, 10403−10410.
25. Overman, S. A., Tsuboi, M., and Thomas, G. J., Jr. (1996) *J. Mol. Biol. 259*, 331−336.
26. Takeuchi, H., Matsuno, M., Overman, S. A., and Thomas, G. J., Jr. (1996) *J. Am. Chem. Soc. 118*, 3498−3507.
27. Matsuno, M., Takeuchi, H., Overman, S. A., and Thomas, G. J., Jr. (1998) *Biophys. J. 74*, 3217−3225.
28. Tsuboi, M., Ushizawa, K., Nakamura, K., Benevides, J. M., Overman, S. A., and Thomas, G. J., Jr. (2001) *Biochemistry 40*, 1238−1247.
29. Tsuboi, M., and Thomas, G. J., Jr. (1997) *Appl. Spectrosc. Rev. 32*, 263−299.
30. Tuma, R., and Thomas, G. J., Jr. (2002) Applications in Life, Pharmaceutical, and Natural Sciences, in *Handbook of Vibrational Spectroscopy 5* (Chalmers, J. M., and Griffiths, P. R., Eds.) pp 3519−3535, John Wiley & Sons, Chichester, U.K.
31. Fritzsche, H., Cross, T. A., Opella, S. J., and Kallenbach, N. R. (1981) *Biophys. Chem. 14*, 283−291.
32. Aubrey, K. L., and Thomas, G. J., Jr. (1991) *Biophys. J. 61*, 1337−1349.
33. Overman, S. A., and Thomas, G. J., Jr. (1995) *Biochemistry 34*, 5440−5451.
34. Overman, S. A., and Thomas, G. J., Jr. (1998) *Biochemistry 37*, 5654−5665.
35. Overman, S. A., and Thomas, G. J., Jr. (1999) *Biochemistry 38*, 4018−4027.
36. Arp, Z., Autrey, D., Laane, J., Overman, S. A., and Thomas, G. J., Jr. (2001) *Biochemistry 40*, 2522−2529.
37. Berkowitz, S. A., and Day, L. A. (1976) *J. Mol. Biol. 102*, 531−547.
38. Sutherland, G. B. B. M., and Tsuboi, M. (2001) *Proc. R. Soc. London, Ser. A 239*, 446−463.
39. Wilser, W. T., and Fitchen, D. B. (1975) *J. Chem. Phys. 62*, 720−724.
40. Benevides, J. M., Tsuboi, M., Wang, A. H. J., and Thomas, G. J., Jr. (1993) *J. Am. Chem. Soc. 115*, 5351−5359.
41. Higgs, P. W. (1953) *Proc. R. Soc. London, Ser. A 220*, 472−485.
42. Zbinden, R. (1964) *Infrared Spectroscopy of High Polymers* Academic Press, New York.
43. Thomas, G. J., Jr., and Murphy, P. (1975) *Science 188*, 1205−1207.
44. Bandekar, J. (1992) *Biochim. Biophys. Acta 1120*, 123−143.
45. Thomas, G. J., Jr. (1985) *Spectrochim. Acta 41A*, 217−221.
46. Lee, S.-H., and Krimm, S. (1998) *Biopolymers 46*, 283−317.
47. Siamwiza, M. N., Lord, R. C., Chen, M. C., Takamatsu, T., Harada, I., Matsuura, H., and Shimanouchi, T. (1975) *Biochemistry 14*, 4870−4876.
48. Takeuchi, H., Watanabe, N., and Harada, I. (1988) *Spectrochim. Acta 44A*, 749−761.
49. Tsuboi, M., Ezaki, Y., Aida, M., Suzuki, M., Yimit, A., Ushizawa, K., and Ueda, T. (1998) *Biospectroscopy 4*, 61−71.
50. Lord, R. C., and Thomas, G. J., Jr. (1967) *Spectrochim. Acta 23A*, 2551−2591.
51. Benevides, J. M., and Thomas, G. J., Jr. (1983) *Nucleic Acids Res. 11*, 5747−5761.
52. Nishimura, Y., Tsuboi, M., and Sato, T. (1984) *Nucleic Acids Res. 12*, 6901−6908.
53. Thomas, G. J., Jr. (1986) in *Spectroscopy of Biological Systems* (Clark, R. J. H., and Hester, R. E., Eds.) pp 233−309, John Wiley and Sons, London.
54. Benevides, J. M., Wang, A. H. J., van der Marel, G. A., van Boom, J. H., and Thomas, G. J., Jr. (1988) *Biochemistry 27*, 931−938.
55. Thomas, G. J., Jr., and Tsuboi, M. (1993) in *Advances in Biophysical Chemistry 3* (Bush, C. A., Ed.) pp 1−70, JAI Press Inc., Greenwich, CT.
56. Thomas, G. J., Jr., and Benevides, J. M. (1985) *Biopolymers 24*, 1101−1105.
57. Tsuboi, M. (1962) *J. Polymer Sci. 59*, 139−153.
58. Miyazawa, T. (1960) *J. Chem. Phys. 32*, 1647−1652.
59. Tsuboi, M., Ikeda, T., and Ueda, T. (1991) *J. Raman Spectrosc. 22*, 619−626.
60. Marvin, D. A., Bryan, R. K., and Nave, C. (1987) *J. Mol. Biol. 193*, 315−343.
61. Gonzalez, A., Nave, C., and Marvin, D. A. (1995) *Acta Crystallogr., Sect. D: Biol. Crystallogr. 51*, 792−804.
62. Shon, K. J., Kim, Y., Colnago, L. A., and Opella, S. J. (1991) *Science 252*, 1303−1305.
63. Ueda, T., Ushizawa, K., and Tsuboi, M. (1996) *J. Mol. Struct. 319*, 171−187.
64. Wen, Z. Q., and Thomas, G. J., Jr. (2000) *Biochemistry 39*, 146−152.
65. Wen, Z. Q., Overman, S. A., Bondre, P., and Thomas, G. J., Jr. (2001) *Biochemistry 40*, 449−458.
66. Overman, S. A., Aubrey, K. L., Vispo, N. S., Cesareni, G., and Thomas, G. J., Jr. (1994) *Biochemistry 33*, 1037−1042.
67. Thomas, G. J., Jr., Benevides, J. M., Overman, S. A., Ueda, T., Ushizawa, K., Saitoh, M., and Tsuboi, M. (1995) *Biophys. J. 68*, 1073−1088.
68. Tsuboi, M., Ueda, T., Ushizawa, K., Ezaki, Y., Overman, S. A., and Thomas, G. J., Jr. (1996) *J. Mol. Struct. 379*, 43−50.

BI020566V